Pathways and reduced-dimension five-dimensional potential energy surface for the reactions $H_3^+ + CO \rightarrow H_2 + HCO^+$ and $H_3^+ + CO \rightarrow H_2 + HOC^+$

Hui Li,[1,a)] Tsuneo Hirano,[1,2] Takayoshi Amano,[1] and Robert J. Le Roy[1,b)]
[1]*Department of Chemistry, University of Waterloo, Waterloo, Ontario N2L 3G1, Canada*
[2]*Department of Chemistry, Faculty of Science, Ochanomizu University, Tokyo 112-8610, Japan*

(Received 23 September 2008; accepted 7 November 2008; published online 29 December 2008)

To obtain theoretical insight regarding the stability and formation dynamics of the interstellar ions HCO^+ and HOC^+, stationary points and the associated vibrational frequencies on the full nine-dimensional potential energy surface for the electronic ground state have been calculated using coupled-cluster theory with both single and double substitutions (CCSD). The energetics were refined with a higher-level coupled-cluster method CCSD(T), with core-valence electron correlation treated at the complete basis set limit. To elucidate the formation mechanism and internal relaxation processes, the reaction paths for the reactions $H_3^+ + CO \rightarrow H_2 + HCO^+$ and $H_3^+ + CO \rightarrow H_2 + HOC^+$ were calculated at the second-order Møller–Plesset (MP2) level, and corresponding single-point energies were obtained at the higher CCSD(T)/aug-cc-pVTZ level. Based on the analysis of the main reaction processes, a reduced-dimension five-dimensional potential energy surface for this system was constructed from 128 440 *ab initio* points calculated at the CCSD(T)/aug-cc-pVTZ level. © *2008 American Institute of Physics*. [DOI: 10.1063/1.3041494]

I. INTRODUCTION

The formyl cation HCO^+ was the first molecular ion identified in interstellar space by radio astronomical observations. Since the pioneering work of Woods *et al.*[1] in 1975, HCO^+ has been studied extensively by microwave and infrared spectroscopic techniques.[2–11] The rotational lines in the excited vibrational states have been studied recently up to the 810 GHz band both for HCO^+ and DCO^+ using a terahertz spectrometer, first at Ibaraki University and later at the University of Waterloo.[9,10] Ions were generated in an extended negative glow discharge in a (1:1:13 mTorr) gas mixture of $H_2/CO/Ar$. In those experiments, the rotational lines in high-l states of bending excited states such as (02^20), (03^30), and (04^40) appeared to be weaker than had been expected. Moreover, some low-J lines in (02^20) and (04^20) were observed in emission. These observations clearly indicated that the HCO^+ produced in the extended negative glow discharge was not at thermal equilibrium. The nonthermal population distribution and the local population inversion between the l-doubling components for some low-J levels strongly suggest that HCO^+ is preferentially formed in vibrationally excited C–H stretching states, following a proton hop from H_3^+ to CO, followed by somewhat restrictive relaxation processes subject to preferential selection rules, such as $\Delta l = \pm 1$, and parity selection rules.

The stability of HOC^+, the $[HCO^+]/[HOC^+]$ ratio, and the formation mechanism have been extensively studied for the $H_3^+ + CO$ reaction by both experiment and theory.[12–19] The abundance ratio $[HCO^+]/[HOC^+]$ in interstellar molecular clouds has been found to be 140–360 toward Sgr B2 (OH) and 1800 toward Orion KL.[20,21] In order to explain the observed abundance ratio in dense molecular clouds, the catalytic isomerization reaction $H_2 + HOC^+ \rightleftharpoons H_2 + HCO^+$ has been taken into consideration.[14–16] However, no high-level *ab initio* calculation of the global potential energy surface (PES) for the $H_3^+ + CO$ reaction system has been reported that would elucidate the reaction dynamics.

The object of the present investigation is to provide theoretical insight into the stability and dynamics of the formation of HCO^+ and HOC^+ and of their molecular complexes with H_2. Minimum energy reaction paths (MEPs) for the processes $H_3^+ + CO \rightarrow H_2 + HCO^+$ and $H_3^+ + CO \rightarrow H_2 + HOC^+$ are studied by performing intrinsic reaction coordinate calculations. Molecular configuration changes along the reaction paths are analyzed; this provides important information regarding the dynamics and leads to the construction of a reduced-dimension PES. Finally, a reduced-dimension five-dimensional (5D) PES for the two reactions $H_3^+ + CO \rightarrow H_2 + HCO^+$ and $H_3^+ + CO \rightarrow H_2 + HOC^+$, via both "collinear" and sideways approaches of H_3^+ to CO, is presented.

II. COMPUTATIONAL METHODS

The $H_3^+ + CO$ reaction system can be described in terms of the nine-dimensional (9D) coordinates (R_1, R_2, R_{HH}, R_{CO}, θ_1, θ_2, φ, ϕ_1, and ϕ_2) defined in Fig. 1. Here, R_1 is the distance from the reacting H_1 atom to the center of mass of the terminal H–H group; R_2 is the distance from that reacting H_1 to the center of mass of C–O; R_{HH} and R_{CO} are the terminal H–H and C–O bond lengths, respectively; θ_1 is the angle between the vector pointing from the center of mass of the terminal H–H group to the reacting H_1 atom and the vector pointing from hydrogen H_3 to H_2; θ_2 is the angle between the vector pointing from the center of mass of C–O to the reacting H atom (H_1) and the vector pointing from the oxygen atom to the carbon atom; φ is the angle between the

[a)]Electronic mail: huili@uwaterloo.ca.
[b)]Electronic mail: leroy@uwaterloo.ca.

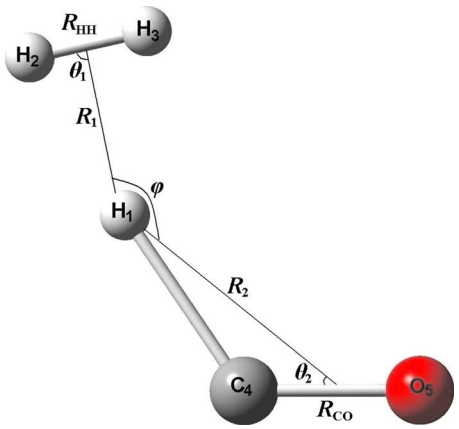

FIG. 1. (Color online) Reaction coordinates for the H_3^++CO system.

vector pointing from atom H_1 to the midpoint of H_2 and H_3 and the vector pointing from atom H_1 to the center of mass of atoms C and O; finally, ϕ_1 and ϕ_2 are two dihedral out-of-plane angles for $C-(H_1H_2H_3)$ and $O-(H_1H_2H_3)$, respectively. Note that throughout this work, we define the "collinear" approach of H_3^+ to CO as a planar process with θ_1 fixed at 90°, φ at 180°, and θ_2 at either 0° or 180°, while what we call a "bending" process concerns planar structures with $\theta_1 = 90°$, while θ_2 varies between 0° and 180°.

Preliminary searches for global minima and transition states (TSs) were carried out at the density functional theory level using Becke's nonlocal three-parameter exchange and correlation functional with the Lee–Yang–Parr correlation functional method (B3LYP),[22,23] and then at the second-order Møller–Plesset (MP2) theory[24–27] level with an augmented correlation-consistent polarized valence triple-ζ (aug-cc-pVTZ) basis set.[28,29] Further optimization of the stationary points and calculations of harmonic normal-mode frequencies were performed to confirm those results using coupled-cluster theory with both single and double substitutions (CCSD)[30,31] while employing the same aug-cc-pVTZ basis sets. Single-point energies at the stationary points determined in this way were then calculated using the higher-level coupled-cluster method with perturbative triples CCSD(T).[31,32] To check for basis set convergence, the stationary points on this PES were calculated with several versions of the augmented correlation-consistent polarized $n\zeta$ basis sets (denoted as aug-cc-pVnZ or aVnZ for $n=3$, 4, and 5).[28,29] The complete basis set limit for valence electrons CBS(V) was estimated by fitting aVnZ energies for different n values to the exponential function of van Mourik *et al.*[33] The core-electron correlation energies were calculated employing a series of correlation-consistent polarized core-valence $n\zeta$ basis sets (denoted as cc-pCVnZ or CVnZ for $n=3$, 4, and 5)[34] and extrapolated to the complete basis set limit CBS(C) using the extrapolation method mentioned above.[33] Finally, the all-electron correlation at the complete basis limit CBS(V+C) was obtained as a sum of the energies of CBS(V) and CBS(C) using the detailed strategy described in Ref. 35. To check for the effect of coupling from excited electronic states, the six lowest states along the MEP for the collinear reaction $H_3^+ + CO \rightarrow H_2 + HCO^+$ were explored by performing state-averaged complete active space self-consistent-field (CASSCF) calculations with equal weights using the aug-cc-pVTZ basis sets. Twelve active electrons and 11 active orbitals were used, including one orbital for each hydrogen, four for carbon, and four for oxygen. Two inactive orbitals that correlate to the core (1s) orbitals of the carbon and oxygen atoms were fully optimized while being constrained to be doubly occupied and excluded from the full valence active space, which is denoted as CASSCF(12,11).

All MEPs, both on the full 9D and the reduced-dimension 5D potential surfaces (see below), were calculated using the quadratic steepest descent method of Sun and Ruedenberg[36] with a step size of 0.1 a_0 amu$^{1/2}$ at the MP2/aug-cc-pVTZ level. Single-point energies were calculated along these MEPs at the CCSD(T)/aug-cc-pVTZ level. MEPs leading from the TS to the complexes of HCO^+ or HOC^+ with H_2 were followed along the "transition vector" of the smallest negative eigenvalue. MEPs for the 'collinear' reaction of H_3^++CO leading directly to the energetically more stable $H_2\cdots HCO^+$ or $H_2\cdots HOC^+$ complexes were first optimized at fixed large intermolecular distances of $R_2=8.0$ and 6.0 Å, respectively, with the other coordinates being free. The initial reactions governed by the attractive forces occurred only along the R_2 coordinate. On examining the MEPs on the full 9D surface, we find that R_{CO} never changes by more than 0.024 Å, the angle θ_1 always lies within 1° of 90°, and the dihedral out-of-plane angles are always within 1° of planarity. We therefore conclude that it would be a very good approximation to describe all of these processes using a reduced-dimension 5D PES, $V(R_1, R_2, R_{HH}, \theta_2, \varphi)$. A surface of this dimension consisting of 128 440 *ab initio* points calculated at the CCSD(T)/aug-cc-pVTZ level was constructed. Stationary-point optimizations were carried out using the *ab initio* quantum chemistry program package GAUSSIAN 03,[37] while CCSD numerical harmonic frequencies and single-point energies were computed using the MOLPRO 2006.1 *ab initio* molecular orbital program package.[38] In the CCSD and CCSD(T) calculations using the aug-cc-pVnZ basis sets, the core electrons were treated as frozen.

III. RESULTS AND DISCUSSION

A. Geometries and energy

The optimized stationary-point geometries on the lowest singlet H_3CO^+ PES are displayed in Fig. 2. As seen there, the equilibrium bond lengths optimized at the B3LYP, MP2, and CCSD levels give consistent results, except for the weak van der Waals bonds of $H_2\cdots HCO^+$ at the B3LYP level and of $H_2\cdots HOC^+$ at the MP2 level of theory. As expected, equilibrium bond lengths optimized at the higher-order CCSD level are usually closest to the experimental values for the H_2, CO, H_3^+, and HCO^+ molecules.[39–41] Our final geometries were determined at the CCSD/aug-cc-pVTZ level. Bending TSs for the isomerization reactions $HOC^+ \rightleftharpoons HCO^+$ and $H_2\cdots HOC^+ \rightleftharpoons H_2\cdots HCO^+$ were obtained at all three levels of theory.

Single-point energies at these stationary points were calculated at the highest level of theory considered herein, CCSD(T), with core-valence basis sets from aCVTZ to aCV5Z and extrapolation to the estimated CBS(V+C) limit,

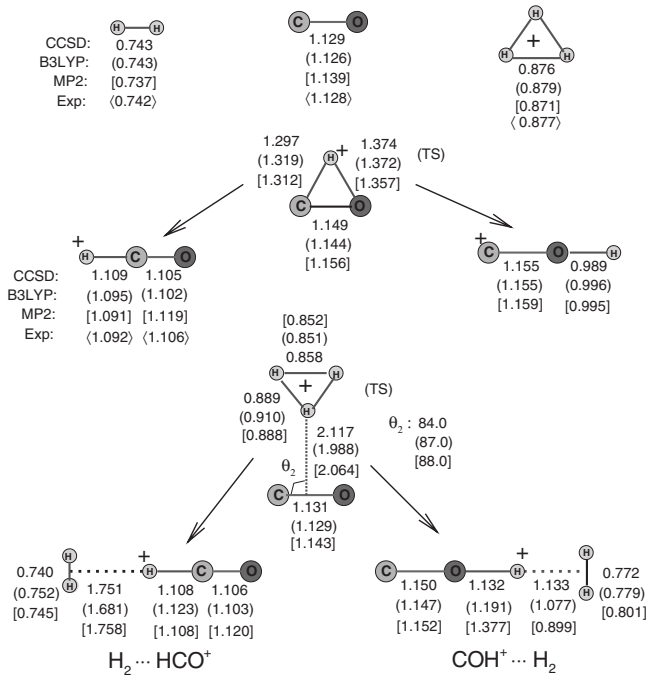

FIG. 2. Optimized geometries of stationary points on the PES for the reactions H_3^++CO→H_2+HCO^+, H_3^++CO→H_2+HOC^+, and H_2+HOC^+⇌H_2 +HCO^+ obtained using the B3LYP, MP2, and CCSD methods (separately) with aug-cc-pVTZ basis sets, compared with experimental values where available, where lengths are in Å and angles in degree. Values at the CCSD level are given as plain numbers, those at the B3LYP level in parentheses, and those at the MP2 level in square brackets, while experimental values are between angled brackets.

as presented in Table I. It is clearly shown there that the total energies tend to converge to well-defined asymptotic limits. Without zero-point energy corrections (ZPE), the barrier height of the $H_3^+\cdots$CO TS complex for the H_2-catalyzed isomerization process $H_2\cdots HOC^+ \rightleftharpoons H_2\cdots HCO^+$ lies below the H_2+HOC^+ asymptotic limit, and the difference increases on increasing the basis set level from aCVTZ to aCV5Z. The estimated energy of this TS at the CBS(V+C) level is −2.198 kcal/mol, which is lower than the previous theoretical value of Herbst and Woon[14] (−1.5 kcal/mol). However, at the CBS(V+C) level, on including the zero-point energy correction, the energy of the $H_3^+\cdots$CO TS complex relative to the H_2+HOC^+ asymptotic limit becomes positive with the value of 0.742 kcal/mol, which is lower than that of Herbst and Woon[14] (1.4 kcal/mol). Other relative energies determined in the present study and a comparison with previous theoretical values[14,16,17] are summarized in Table I.

A schematic energy diagram, without and with zero-point energy corrections for the reactions

$$H_3^+ + CO \rightarrow H_2 + HCO^+, \tag{1}$$

$$H_3^+ + CO \rightarrow H_2 + HOC^+, \tag{2}$$

$$H_2 + HOC^+ \rightleftharpoons H_2 + HCO^+ \tag{3}$$

with zero-point corrected values in parentheses, is shown in Fig. 3. As seen there, reaction (1) is exothermic with a reaction enthalpy change of −40.427 kcal/mol. There are two possible pathways for this reaction. Following a direct proton hop from H_3^+ to CO forming the collinear intermediate complex $H_2\cdots HCO^+$, this complex dissociates to H_2+HCO^+ products, steps labeled as P_1 and P_5 in Fig. 3. Another possible reaction pathway is to first form a metastable bending TS $H_3^+\cdots$CO at θ_2=90° with a reaction enthalpy change of −1.942 kcal/mol, then to proceed to the collinear intermediate complex $H_2\cdots HCO^+$, and finally to dissociate to H_2 +HCO^+ products, steps that are labeled P_2, P_{3a}, and P_5 in Fig. 3.

Reaction (2) is also exothermic, with a small enthalpy change of −2.684 kcal/mol. Two pathways similar to those for reaction (1) are seen in Fig. 3. One is direct proton transfer from H_3^+ to CO via the collinear intermediate complex $H_2\cdots HOC^+$, followed by dissociation to H_2+HOC^+ products, paths that are labeled P_4 and P_6. The other is to form

TABLE I. Calculated energies (in kcal mol^{-1}) on the ground-state PES obtained at the CCSD(T) level of theory using various basis sets, all expressed relative to the energy at the H_3^++CO reactant asymptote. See text for notations regarding the *ab initio* calculation methods and basis sets (*a*: basis set $(11s7p1d/6s1p)/[5s4p1d/3s1p]$ and *b*: basis set 6-311++G(*df*,*pd*)).

		Asymptote for H_2 with:			Complex		
Levels	Ref.	HCO^+	HCO^+ (TS)	HOC^+	$H_2\cdots HCO^+$	$H_3^+\cdots$CO (TS)	$H_2\cdots HOC^+$
CCSD(T)/aVTZ	Present	−41.481	34.761	−2.001	−45.899	−3.386	−15.428
CCSD(T)/aVQZ	Present	−41.176	35.318	−1.604	−45.474	−3.257	−14.921
CCSD(T)/aV5Z	Present	−40.981	35.563	−1.339	−45.240	−3.167	−14.636
CCSD(T)/CBS(V)	Present	−40.867	35.706	−1.185	−45.105	−3.115	−14.471
CCSD(T)/aCVTZ	Present	−41.752	34.935	−1.872	−46.074	−3.368	−15.334
CCSD(T)/aCVQZ	Present	−41.396	35.562	−1.353	−45.695	−3.229	−14.726
CCSD(T)/aCV5Z	Present	−41.214	35.826	−1.057	−45.474	−3.137	−14.417
CCSD(T)/CBS(V+C)	Present	−41.108	35.979	−0.885	−45.345	−3.083	−14.238
CCSD(T)/cc-pVTZ	14	−41.0		−1.6	−45.2	−3.1	−15.0
CCSD(T)/CBS(V+C)+ZPE	Present	−40.427	32.295	−2.684	−42.977	−1.942	−13.748
CCSD(T)/cc-pVTZ+ZPE	14			−3.3		−1.9	−14.8
CISD/*a*+ZPE	17	−38.7		−0.3	−41.2		−6.9
MP4/*b*+ZPE	16	−43.0		−3.0	−45.0	−1.0	−14.0

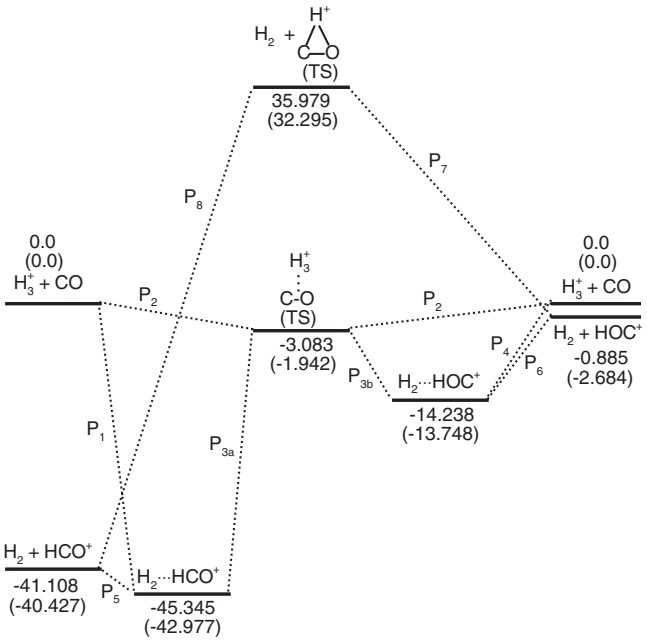

FIG. 3. Schematic energy diagram for the reactions $H_3^+ + CO \rightarrow H_2 + HCO^+$, $H_3^+ + CO \rightarrow H_2 + HOC^+$, and $H_2 + HOC^+ \rightleftharpoons H_2 + HCO^+$ at the CCSD(T)/CBS(V+C) level of theory. The computed relative energies (in kcal mol^{-1}) listed for the stationary points are given both without and with (values in parentheses) zero-point energy corrections.

the metastable bending TS $H_3^+ \cdots CO$, and then proceed through the intermediate collinear complex $H_2 \cdots HOC^+$ to dissociate to $H_2 + HOC^+$ products via the processes labeled P_2, P_{3b}, and P_6.

Isomerization from HOC^+ to HCO^+ via reaction (3) is exothermic with an enthalpy change of −37.743 kcal/mol at the CCSD(T)/CBS(V+C)+ZPE level of theory, a result in good agreement with the previous theoretical value (−37.7 kcal/mol at the CCSD(T)/[TZ2P(f,d)+diff] level) of Yamaguchi *et al.*[19] and with the experimental estimate of McMahon and Kebarle[42] (−36.3 kcal/mol). As shown in Fig. 3, it has two possible channels. On the isolated HOC^+/HCO^+ isomerization pathways, which are labeled P_7 and P_8, there is a TS for proton exchange with a barrier height of 34.979 kcal/mol, a value that also agrees well with the previous theoretical estimate of 34.9 kcal/mol obtained at the CCSD(T)/[TZ2P(f,d)+diff] level[19] and is somewhat lower than the value of 38.9 kcal/mol estimated by Martin *et al.*[43] With H_2 catalysis, by forming the intermediate complex $H_2 \cdots HOC^+$ or $H_2 \cdots HCO^+$ and then proceeding through the metastable bending TS $H_3^+ \cdots CO$, the barrier height for this pathway drops to 0.742 kcal/mol through processes labeled as P_6, P_{3b}, P_{3a}, and P_5.

Reactions (1)–(3) are all exothermic, with two energetically accessible reaction channels for each process. In order to examine them in more detail, MEPs were calculated at the MP2/aug-cc-pVTZ level in order to obtain insight regarding their formation mechanism and internal relaxation processes. Hereafter, we focus on examining paths P_1, P_4, P_{3a}, and P_{3b} one by one, as we believe them to be the most important processes for this system.

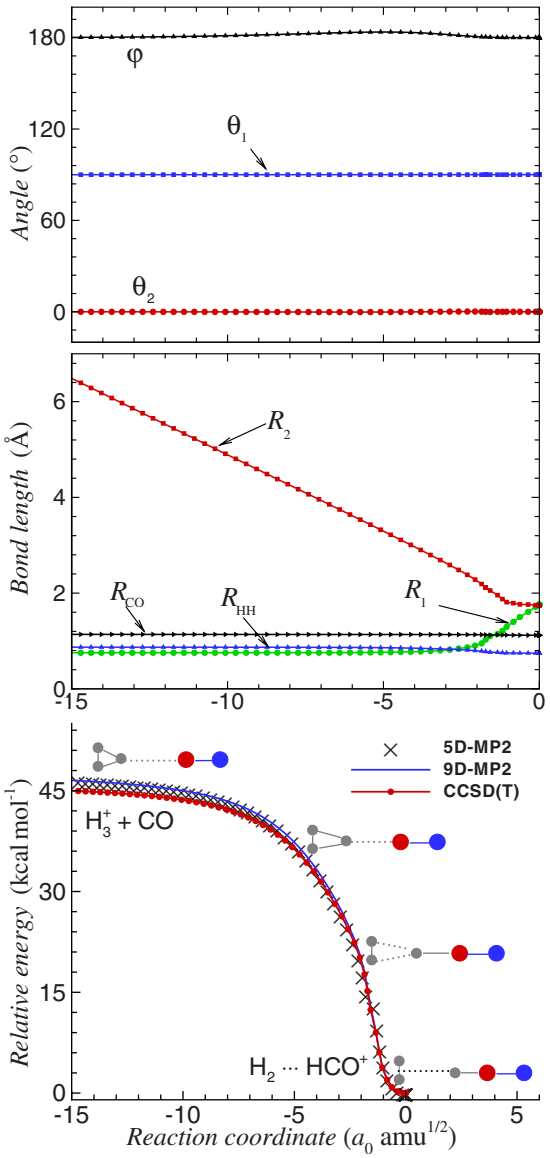

FIG. 4. (Color online) MEP for the collinear $H_3^+ + CO \rightarrow H_2 \cdots HCO^+$ reaction. Changes in geometric parameters shown in two upper segments are those along the MEP on the 9D MP2 PES. The label 5D-MP2 denotes the MEP on the reduced-dimension 5D PES at the MP2 level, 9D-MP2 that on the full 9D MEP at the MP2 level, and CCSD(T) the energy for points on the MEP determined by the 9D-MP2 surface.

B. Minimum energy paths

For all of the MEPs discussed below, the dihedral angles ϕ_1 and ϕ_2 always lie within 1.0° of 180.0°. Thus, most of the following discussion assumes that all atoms always remain in the same plane.

Properties of step P_1 on the first path for reaction (1) are shown in Fig. 4. MEPs were obtained at the MP2/aug-cc-pVTZ level of theory on both the full 9D and reduced 5D surfaces. As seen in the lowest segment of Fig. 4, there is no TS or minimum along this path for either surface. The bond length and angle changes along the MEP on the 9D MP2 PES are shown in the middle and uppermost segments of Fig. 4, respectively. It is clear that the coordinates R_{CO}, R_{HH}, θ_1, θ_2, and φ remain nearly constant along this path, while the changes in R_1 and R_2 are substantial. As R_2 decreases and

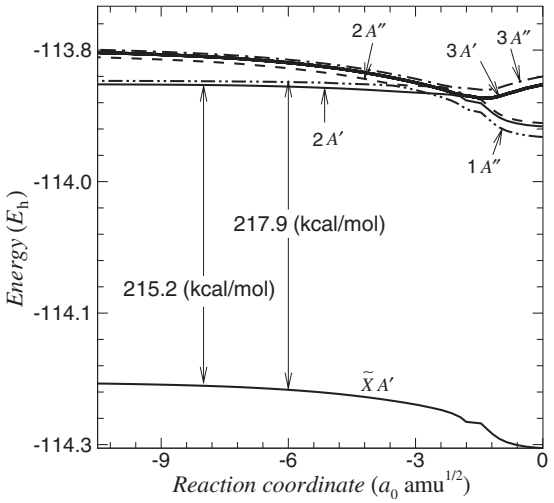

FIG. 5. Energies of the electronic ground state and first five excited states along the 9D MP2 MEP for the collinear ground-state H_3^++CO $\rightarrow H_2\cdots HCO^+$ reaction.

R_1 increases, a proton is transferred directly from H_3^+ to CO via the H_3^+ collinear approach to the carbon end of CO.

To check the MP2 reaction path, CCSD(T) potential energies were calculated along the full 9D MP2 reaction path. It can be seen from the lowest segment of Fig. 4 that CCSD(T) relative energies along the MEP are very similar to the MP2 results. Thus, we assume that the MP2 approach provides a reasonable description of these reaction paths.

In order to test for the effect of coupling from excited electronic states, the energies of the five lowest excited states along the 9D MP2 MEP have been calculated at the CASSCF/aug-cc-pVTZ level of theory, yielding the results shown in Fig. 5. As seen there, along this path the lowest excited states of A' and A'' symmetries lie 215.2 and 217.9 kcal/mol above the ground state, respectively. These energy gaps are so large that the effects of excited states should be very small.

The properties of the MEP for step P_4 of reaction (2) are shown in Fig. 6, with the energy for this formation process displayed in the lowest segment. MEPs obtained at the MP2/aug-cc-pVTZ level on both the 9D and 5D surfaces indicate clearly that there is also no barrier or minimum along this path. Although the relative energies obtained with the more accurate CCSD(T) method are somewhat different from the MP2 results, the topology of their MEPs is quite consistent. It can be seen from the middle and uppermost segments of Fig. 6 that along the 9D MP2 MEP the coordinates R_{CO}, R_{HH}, θ_1, θ_2, and φ are again nearly constant, with the first three remaining very near the free-molecule equilibrium values, while changes in R_1 and R_2 again characterize the progress of the reaction. With decreases in R_2 and increases in R_1, a proton is transferred directly from H_3^+ to CO via the H_3^+ collinear approach to the oxygen end of CO. Note that R_1 (1.133 Å) in the resulting $H_2\cdots HOC^+$ complex is much shorter than R_1 (1.751 Å) in the $H_2\cdots HCO^+$ complex.

Properties of the portion of the pathways for reaction (3) involving the isomerization processes of steps P_{3a} and P_{3b} are shown in Fig. 7. MEPs leading from the high-energy $H_3^+\cdots CO$ TS complex to the energetically more stable species $H_2\cdots HCO^+$ and $H_2\cdots HOC^+$ are obtained at the MP2/aug-cc-pVTZ level of theory on both the 9D and 5D potentials. It can be seen from the lowest segment of Fig. 7 that the relative energies along the MEP on both the full 9D and the 5D MP2 surfaces are practically indistinguishable and that the CCSD(T) results along the 9D MEPs are also in fairly good agreement with these MP2 results. As shown in the middle segment of Fig. 7, along the 9D MP2 MEPs from $H_2\cdots HCO^+$ via the $H_3^+\cdots CO$ TS to $H_2\cdots HOC^+$, R_2 and R_{HH} first increase and then decrease after passing the TS, while R_1 varies in the opposite direction, first decreasing and then increasing after passing the TS. The R_{CO} value always remains very near the average bond length for ground-state gas phase CO. The uppermost segment of Fig. 7 displays the changes in angle along these 9D MP2 MEPs. The isomerization between the collinear entrance and exit channel complexes $H_2\cdots HCO^+$ and $H_2\cdots HOC^+$ occurs via a bending TS

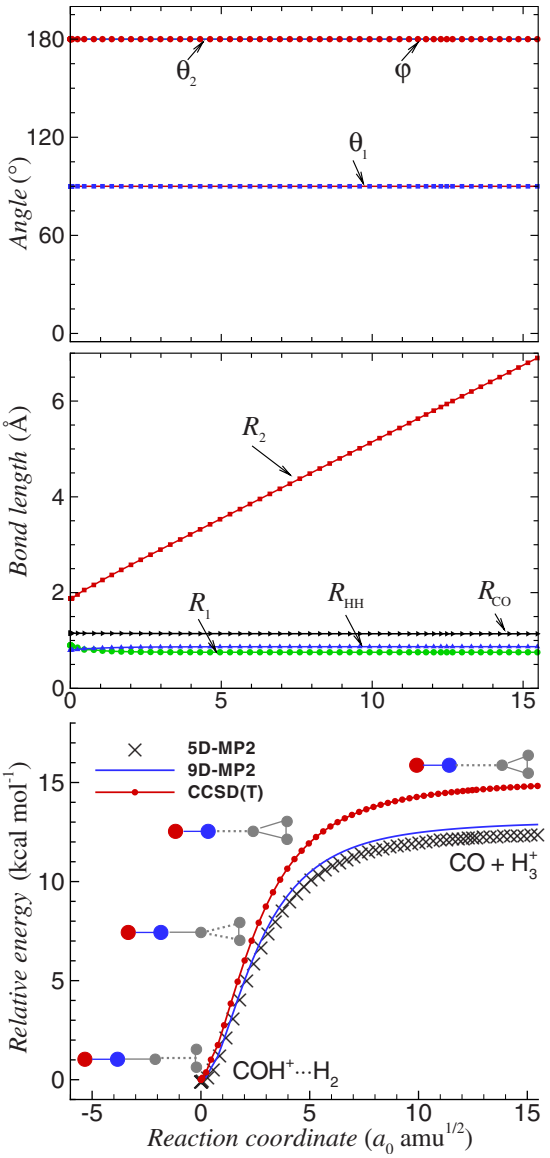

FIG. 6. (Color online) MEP for the collinear H_3^++CO$\rightarrow H_2\cdots HOC^+$ reaction. Changes in geometric parameters shown in the two upper segments are those along the MEP on the 9D MP2 PES, while the labels 5D-MP2, 9D-MP2, and CCSD(T) are defined as in Fig. 4.

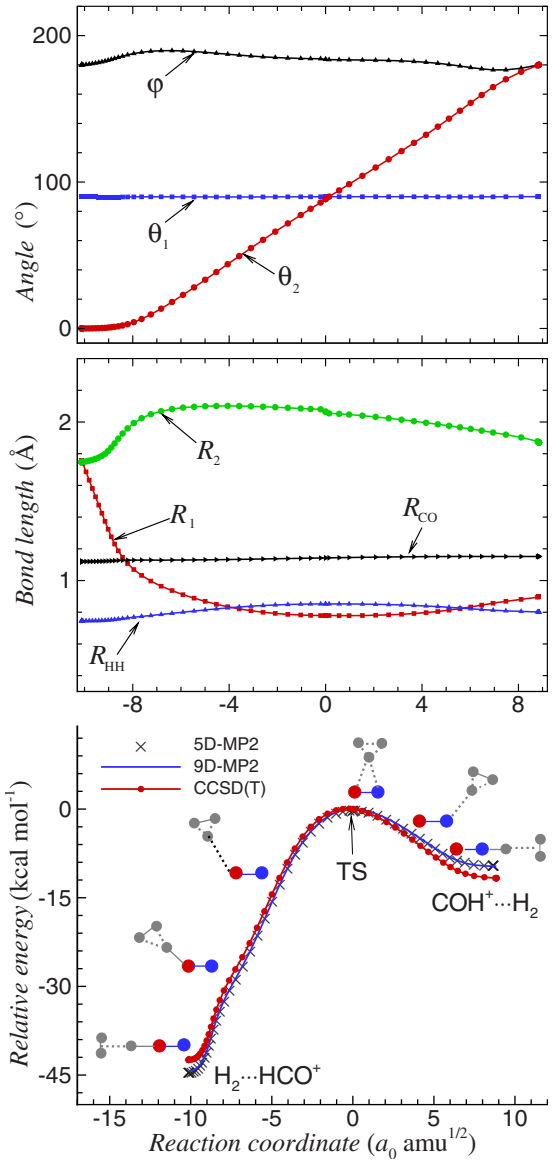

FIG. 7. (Color online) MEP for the $H_2\cdots HCO^+ \leftarrow H_3^+\cdots CO$ (TS) $\rightarrow H_2\cdots HOC^+$ bending reactions. Changes in geometric parameters shown in the two upper segments are those along the MEP on the 9D MP2 PES, while the labels 5D-MP2, 9D-MP2, and CCSD(T) are defined as in Fig. 4.

of $H_3^+\cdots CO$, while θ_2 varies from 0.0° to 180.0°. The angle φ has small changes along these MEPs, and θ_1 always remains very close to 90.0°.

To summarize the above MEP analyses, we note that the reactions mostly involve changes in the three bond lengths R_1, R_2, and R_{HH} and the two angles θ_2 and φ, with very small changes in θ_1 and R_{CO}, and that it is a very good approximation to fix θ_1 at 90.0° and R_{CO} at the average value for the ground-state CO molecule. As mentioned above, the two dihedral angles for $C-(H_1H_2H_3)$ and $O-(H_1H_2H_3)$ are always planar for all MEPs, so we can perform our calculations in the C_s symmetry framework. Thus, we conclude that the reduced-dimension 5D PES $V(R_1, R_2, R_{HH}, \theta_2, \varphi)$ for the H_3CO^+ system suffices to represent all reaction processes of interest. The close agreement of the MP2 results obtained on the 9D and 5D PESs, as shown in the lowest segments of Figs. 4, 6, and 7, indicates that this approximation of using a reduced-dimension 5D PES is reasonable.

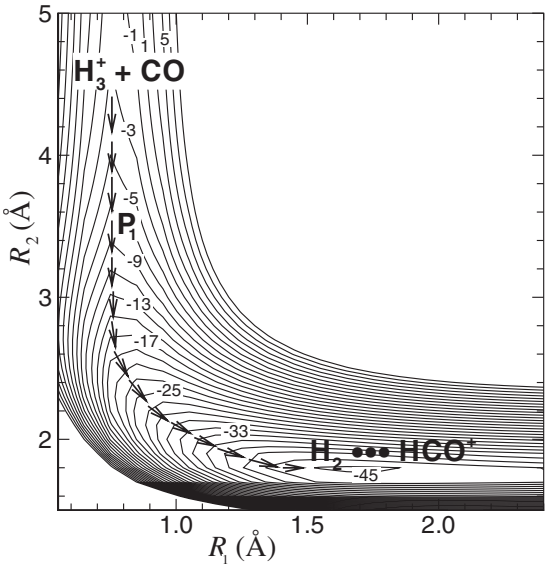

FIG. 8. Contour plot for the planar $H_3^+ + CO \rightarrow H_2 + HCO^+$ collinear ($\theta_2 = 0°$, $\theta_1 = 90°$, and $\varphi = 180°$) reaction calculated at the CCSD(T)/aug-cc-pVTZ level, showing the dependence of the PES on coordinates R_1 and R_2 with R_{HH} being optimized. The relative contour energies are in kcal/mol.

C. Potential energy surface

Based on the discussion in the previous section, we constructed a reduced-dimension 5D PES to account for the most important channels for reactions (1)–(3). We chose relatively dense grids for coordinates R_1, R_2, and R_{HH}: 13 points from 0.55 to 2.5 Å for R_1, 19 points from 1.5 to 10.0 Å for R_2, and 5 points from 0.6 to 1.17 Å for R_{HH}. For the bending coordinates θ_2 and φ, we adopted grids consisting of 13 points for θ_2 ranging from 0 to 180° at intervals of 15° and 8 points for φ ranging from 130 to 250° at the same intervals of 15°. This yielded a total of 128 440 points. The C–O bond length was fixed at the experimental average bond length of a ground-state CO molecule, $r_0 = 1.1309$ Å.[44] 5D spline interpolation was used to generate values of the potential energy between the grid points.

Figures 8 and 9 present contour plots of PESs for processes P_1 and P_4 for the collinear reactions (1) and (2), respectively. They show the dependence of the PES on R_1 and R_2, with the R_{HH} distance optimized at every $\{R_1, R_2\}$ point on each surface and with θ_1 fixed at 90.0° and φ fixed at 180.0°, while θ_2 is fixed at 0.0° or 180.0° for reactions (1) and (2), respectively. As seen in Figs. 8 and 9, there exists a minimum on each PES corresponding to the $H_2\cdots HCO^+$ or $H_2\cdots HOC^+$ complex, with the two terminal hydrogens H_2 and H_3 aligned perpendicular to the HCO^+ or HOC^+ axis, respectively. However, there is no barrier to reaction along these collinear paths and no local minimum corresponding to a $H_3^+\cdots CO$ complex. Rather, the end-on approach of H_3^+ to CO at the carbon or oxygen end of CO goes directly to a minimum corresponding to the $H_2\cdots HCO^+$ or $H_2\cdots HOC^+$ complex, respectively. With further increases in R_1, the $H_2\cdots HCO^+$ and $H_2\cdots HOC^+$ complexes dissociate to their corresponding asymptotic limits of $H_2 + HCO^+$ and $H_2 + HOC^+$, respectively, through the processes labeled as P_5 and P_6 in Fig. 3. The $H_2\cdots HCO^+$ complex has been experi-

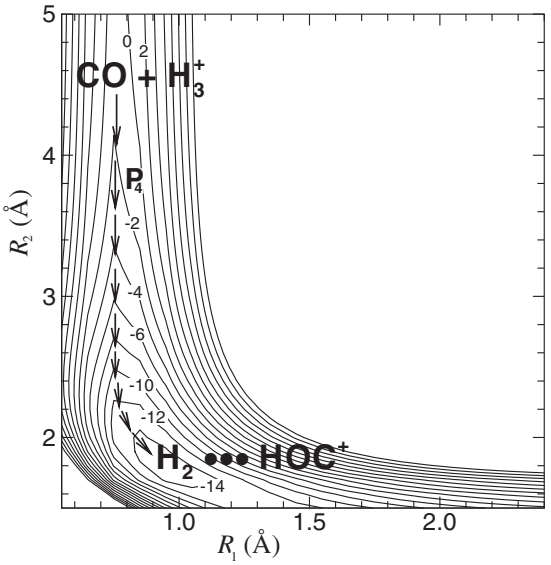

FIG. 9. Contour plot for the $H_3^+ + CO \rightarrow H_2 + HOC^+$ collinear ($\theta_2 = 180°$, $\theta_1 = 90°$, and $\varphi = 180°$) reaction calculated at the CCSD(T)/aug-cc-pVTZ level, showing the dependence of the PES on coordinates R_1 and R_2 with R_{HH} being optimized. The relative contour energies are in kcal/mol.

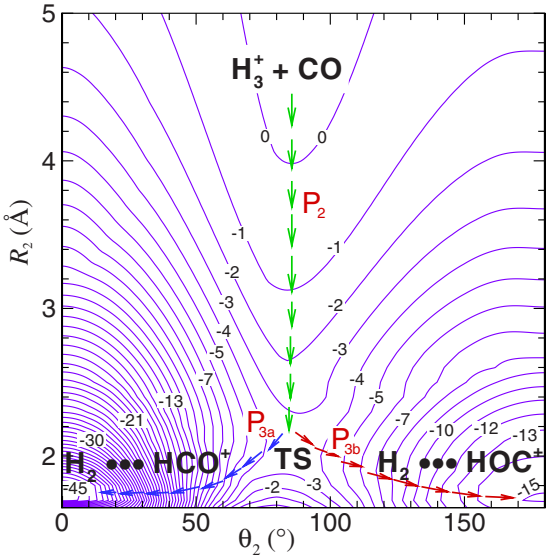

FIG. 10. (Color online) Contour plot for the $H_2 \cdots HCO^+ \leftarrow H_3^+ \cdots CO$ (TS) $\rightarrow H_2 \cdots HOC^+$ bending reactions calculated at the CCSD(T)/aug-cc-pVTZ level, showing the dependence of the PES on θ_2 and R_2 with R_1, R_{HH}, and φ being optimized. The relative contour energies are in kcal/mol.

mentally detected in the infrared vibrational predissociation spectra,[45] but $H_2 \cdots HOC^+$ has not yet been observed.

As seen in Fig. 8, the equilibrium structure for the complex $H_2 \cdots HCO^+$ is located at $R_1 = 1.755$ Å, $R_2 = 1.751$ Å, and $R_{HH} = 0.764$ Å, values in good agreement both with those ($R_1 = 1.751$ Å, $R_2 = 1.740$ Å, and $R_{HH} = 0.740$ Å) obtained by performing full 9D optimization at the CCSD/aug-cc-pVTZ level of theory and with previous theoretical values ($R_1 = 1.744$ Å, $R_2 = 1.745$ Å, and $R_{HH} = 0.751$ Å) calculated at the QCISD(T)/6-311G($2df$,$2pd$) level of theory.[45] The potential minimum is −46.197 kcal/mol below the asymptotic limit of $H_3^+ + CO$; this energy difference is in good agreement with the value (−45.899 kcal/mol) obtained at the CCSD(T)/aVTZ level, and slightly smaller than that (−45.345 kcal/mol) obtained at the CCSD(T)/CBS(V+C) level, as shown in Table I.

Figure 9 shows that the equilibrium structure for the complex $H_2 \cdots HOC^+$ is located at $R_1 = 0.995$ Å, $R_2 = 1.735$ Å, and $R_{HH} = 0.789$ Å, values that are consistent with those ($R_1 = 1.133$ Å, $R_2 = 1.625$ Å, and $R_{HH} = 0.772$ Å) obtained at the CCSD/aug-cc-pVTZ level of theory with the full 9D potential. This potential minimum lies 15.411 kcal/mol below the $H_3^+ + CO$ asymptote; this energy difference is in agreement with the difference (15.428 kcal/mol) obtained at the CCSD(T)/aVTZ level and slightly smaller than that (14.238 kcal/mol) obtained at the CCSD(T)/CBS(V+C) level, as seen in Table I.

Figure 10 displays contour plots of the PES for the sideways-approach $H_3^+ + CO \rightarrow H_2 \cdots HCO^+$ and $H_3^+ + CO \rightarrow H_2 \cdots HOC^+$ bending channel reactions, showing the dependence of the PES on θ_2 and R_2, with R_1, R_{HH}, and φ being optimized. This figure makes it clear that the isomerization process via steps P_{3a} and P_{3b} is hindered by a barrier. The saddle point of this barrier lies at $R_1 = 0.777$ Å, $R_2 = 2.069$ Å, $R_{HH} = 0.840$ Å, $\theta_2 = 86.0°$, and $\varphi = 186.0°$, values that are consistent with those ($R_1 = 0.780$ Å, $R_2 = 2.117$ Å, $R_{HH} = 0.858$ Å, $\theta_2 = 84.0°$, and $\varphi = 187.0°$) obtained by performing full 9D optimization at the CCSD/aug-cc-pVTZ level of theory, as listed in Fig. 2. This TS also lies 3.691 kcal/mol below the asymptotic $H_3^+ + CO$ limit, as shown by process P_2 in Fig. 10. This energy difference is consistent with the value of 3.386 kcal/mol calculated at the CCSD(T)/aVTZ level and slightly larger than the 3.083 kcal/mol obtained at the CCSD(T)/CBS(V+C) level of theory, as shown in Table I. Our grid of 128 440 potential function values may be obtained from the authors or from the journal's supplementary data archive.[46]

IV. CONCLUSION

We report a reduced-dimension 5D global *ab initio* PES for reactions on the ground electronic state surface for the H_3CO^+ system, consisting of 128 440 points obtained at the CCSD(T)/aug-cc-pVTZ level of theory. This surface includes all possible pathways for the reactions $H_3^+ + CO \rightarrow H_2 + HCO^+$ and $H_3^+ + CO \rightarrow H_2 + HOC^+$ and for the hydrogen-catalyzed isomerization process $H_2 + HOC^+ \rightleftharpoons H_2 + HCO^+$. Our results indicate that there are two pathways for each of the $H_3^+ + CO \rightarrow H_2 + HCO^+$ and $H_3^+ + CO \rightarrow H_2 + HOC^+$ reactions: direct proton transfer via the collinear approach from the carbon or oxygen end of CO and a bending reaction channel associated with sideways approach through a $H_3^+ \cdots CO$ TS complex. This TS is also an important step in the hydrogen-catalyzed isomerization process $H_2 + HOC^+ \rightleftharpoons H_2 + HCO^+$ via the formation of a $H_2 \cdots HOC^+$ or $H_2 \cdots HCO^+$ collinear complex, followed by dissociation to the product $H_2 + HOC^+$ or $H_2 + HCO^+$. The formation and dissociation processes described on the 5D global PES (Sec. III C) are consistent with the MEP analysis (Sec. III B), which was initially explored at the MP2/aug-cc-pVTZ level for both 9D and 5D optimizations. Stationary-point geometries and relative energies have been refined at the CCSD(T) level with core-electron correlation at the CBS limits, which

are in good agreement with available experimental results. We are planning to fit our PES to an analytic form and to perform quantum dynamics study for these reactions.

[1] R. C. Woods, T. A. Dixon, R. J. Saykally, and P. G. Szanto, Phys. Rev. Lett. **35**, 1269 (1975).
[2] M. Bogey, C. Demuynck, and J. L. Destombes, Mol. Phys. **43**, 1043 (1981).
[3] C. S. Gudeman, M. H. Begemann, J. Pfaff, and R. J. Saykally, Phys. Rev. Lett. **50**, 727 (1983).
[4] T. Amano, J. Chem. Phys. **79**, 3595 (1983).
[5] S. C. Foster, A. R. W. McKellar, and T. J. Sears, J. Chem. Phys. **81**, 578 (1984).
[6] P. B. Davies and W. J. Rothwell, J. Chem. Phys. **81**, 5239 (1984).
[7] F. Tinti, L. Bizzocchi, C. D. Esposti, and L. Dore, Astrophys. J. Lett. **669**, L113 (2007).
[8] V. Lattanzi, A. Walters, B. J. Drouin, and J. C. Pearson, Astrophys. J. **662**, 771 (2007).
[9] T. Hirao, S. Yu, and T. Amano, J. Chem. Phys. **127**, 074301 (2007).
[10] T. Hirao, S. Yu, and T. Amano, J. Mol. Spectrosc. **248**, 26 (2008).
[11] C. F. Neese, C. M. Lindsay, T. Oka, P. S. Kreynin, and I. R. McNab, The 60th Ohio State University International Symposium on Molecular Spectroscopy, The Ohio State University, Columbus, OH, 2005: Paper No. MG08.
[12] M. A. Smith, S. Schlemmer, J. von Richthofen, and D. Gerlich, Astrophys. J. Lett. **578**, L87 (2002).
[13] W. Wagner-Redeker, P. R. Kemper, M. F. Jarrold, and M. T. Bowers, J. Chem. Phys. **83**, 1121 (1985).
[14] E. Herbst and D. E. Woon, Astrophys. J. Lett. **463**, L113 (1996).
[15] E. Herbst and D. E. Woon, Astrophys. J. Lett. **471**, L73 (1996).
[16] M. F. Jarrold, M. T. Bowers, D. J. DeFrees, A. D. McLean, and E. Herbst, Astrophys. J. **303**, 392 (1986).
[17] D. A. Dixon, A. Komornicki, and W. P. Kraemer, J. Chem. Phys. **81**, 3603 (1984).
[18] G. E. Moyano, S. A. Jones, and M. A. Collins, J. Chem. Phys. **124**, 124318 (2006).
[19] Y. Yamaguchi, C. A. Richards, Jr., and H. F. Schaefer III, J. Chem. Phys. **101**, 8945 (1994).
[20] L. M. Ziurys and A. J. Apponi, Astrophys. J. Lett. **455**, L73 (1995).
[21] A. J. Apponi and L. M. Ziurys, Astrophys. J. **481**, 800 (1997).
[22] A. D. Becke, J. Chem. Phys. **98**, 5648 (1993).
[23] C. T. Lee, W. T. Yang, and R. G. Parr, Phys. Rev. B **37**, 785 (1988).
[24] C. Møller and M. S. Plesset, Phys. Rev. **46**, 618 (1934).
[25] M. Head-Gordon, J. A. Pople, and M. J. Frisch, Chem. Phys. Lett. **153**, 503 (1988).
[26] M. J. Frisch, M. Head-Gordon, and J. A. Pople, Chem. Phys. Lett. **166**, 275 (1990).
[27] M. J. Frisch, M. Head-Gordon, and J. A. Pople, Chem. Phys. Lett. **166**, 281 (1990).
[28] T. H. Dunning, Jr., J. Chem. Phys. **90**, 1007 (1989).
[29] R. A. Kendall, T. H. Dunning, Jr., and R. J. Harrison, J. Chem. Phys. **96**, 6796 (1992).
[30] J. A. Pople, R. Krishnan, H. B. Schlegel, and J. S. Binkley, Int. J. Quantum Chem. **14**, 545 (1978).
[31] C. Hampel, K. A. Peterson, and H.-J. Werner, Chem. Phys. Lett. **190**, 1 (1992).
[32] M. J. O. Deegan and P. J. Knowles, Chem. Phys. Lett. **227**, 321 (1994).
[33] T. van Mourik, A. K. Wilson, and T. H. Dunning, Jr., Mol. Phys. **96**, 529 (1999).
[34] D. E. Woon and T. H. Dunning, Jr., J. Chem. Phys. **103**, 4572 (1995).
[35] H. Li and R. J. Le Roy, J. Phys. Chem. A **111**, 6248 (2007).
[36] J. Q. Sun and K. Ruedenberg, J. Chem. Phys. **99**, 5269 (1993).
[37] M. J. Frisch, G. W. Trucks, H. B. Schlegel *et al.*, GAUSSIAN 03, Revision A.1, Gaussian, Inc., Pittsburgh, PA, 2003.
[38] MOLPRO, version 2006.1, a package of *ab initio* programs. H.-J. Werner, P. J. Knowles, R. Lindh, F. R. Manby, M. Schütz *et al.*, see http://www.molpro.net.
[39] K. P. Huber and G. Herzberg, *Constants of Diatomic Molecules* (Van Nostrand, New York, 1979).
[40] S. C. Foster, A. R. W. McKellar, I. R. Peterkin, J. K. G. Watson, F. S. Pan, M. W. Crofton, R. S. Altman, and T. Oka, J. Chem. Phys. **84**, 91 (1986).
[41] L. Dore, S. Beninati, C. Puzzarini, and G. Cazzoli, J. Chem. Phys. **118**, 7857 (2003).
[42] T. B. McMahon and P. Kebarle, J. Chem. Phys. **83**, 3919 (1985).
[43] J. M. L. Martin, P. R. Taylor, and T. J. Lee, J. Chem. Phys. **99**, 286 (1993).
[44] G. Winnewisser, S. P. Belov, T. Klaus, and R. Schieder, J. Mol. Spectrosc. **184**, 468 (1997).
[45] E. J. Bieske, S. A. Nizkorodov, F. R. Bennett, and J. P. Maier, J. Chem. Phys. **102**, 5152 (1995).
[46] See EPAPS Document No. E-JCPSA6-129-012848 for an ASCII file containing a complete listing of the 128 440 energies defining reduced-dimension 5D PES for the reactions $H_3^+ + CO \rightarrow H_2 + HCO^+$ and $H_3^+ + CO \rightarrow H_2 + HOC^+$ at the CCSD(T)/aCVTZ level of theory. For more information on EPAPS, see http://www.aip.org/pubservs/epaps.html.